Materials Advances

ROYAL SOCIETY OF CHEMISTRY

COMMUNICATION

View Article Online
View Journal | View Issue



Cite this: *Mater. Adv.*, 2023, 4, 1628

Received 16th February 2023,
Accepted 3rd March 2023

DOI: 10.1039/d3ma00075c

rsc.li/materials-advances

# Composite membranes based on self-crosslinking polyelectrolyte-wrapped ZIF-8/CNT nanoparticles for solar steam evaporation†

Yingying Zhu,‡[a] Hongyu Lan,‡[a] Panpan He,[b] Xiangwei Zhu,[d] Jiang Gong,[b] Zhiyue Dong*[a] and Minghua Zeng*[ac]

**Zeolitic imidazolate frameworks (ZIFs) are widely studied for selective transport of small molecules with their designable channels and cage-like pores. Herein, we design solar-thermal hybrid membrane ZCP-20 (ZIF-8/CNTs@PCMVIMBr-20), where ZIF-8 is used as a water transmission channel. ZIF-8 was integrated with self-crosslinking PCMVIMBr (poly[1-cyanomethyl-3-vinylimidazolium bromide]), where its imidazole moiety coordinates with Zn ions to give a mechanically robust membrane. The hydrophobic channels of ZIF-8 enable the formation of discrete water clusters. Differential scanning calorimetry and dark water evaporation rate evaluation indicate that the water evaporation enthalpy in the ZCP-20 membrane is 1.00 kJ $g^{-1}$. Consequently, the ZCP-20 membrane exhibits a high evaporation rate of 2.48 kg $m^{-2}$ $h^{-1}$ under one sun irradiation and displays stable evaporation rates for 20 h. Remarkably, the ZCP-20 membrane can tolerate various water sources (*e.g.*, dye-polluted water) or even strongly acidic (pH = 1) or basic (pH = 13) solutions.**



With rapid population growth and extensive water pollution, the demand for freshwater resources has increased sharply.[1–5] Solar-thermal steam generation is an energy-efficient water purification technology potentially capable of alleviating the fresh water shortages, which has been widely investigated for producing freshwater from seawater or sewage.[6–10] In order to enhance the water evaporation performance of functional materials, enormous attempts have been devoted to controlling their morphology by creating hierarchical architectures,[11–13] including carbon-based materials,[14–16] metals,[17,18] metal oxides/carbides,[19,20] polymers,[21–23] and porous frameworks.[24–27] The structures of evaporators have been investigated to promote water evaporation by increasing the solar absorbance, heat localization and water transportation.[28–30]

Metal–organic frameworks (MOFs) are porous organic-inorganic hybrid materials, which could be designed and post-synthetically modified to give desirable properties.[31] Zeolitic imidazolate frameworks (ZIFs) are a special class of MOFs[32–35] with hierarchical ordered porous structures. Thus, ZIFs could be used as templates to produce materials with high solar energy absorption for the reduction of sunlight reflection. As a prototype ZIF, ZIF-8 is an ideal candidate component for constructing hierarchical architectures with low thermal conductivity, enhanced solar harvesting and water transportation.[36–39] ZIF-8 possesses large cavities of 11.6 Å diameter with a small aperture of 3.4 Å, which is suitable for hosting water clusters.[40] The pores are hydrophobic, and thus the equilibrium of water adsorption–desorption could be established quickly to promote water transmission. The water molecules moving into the channels of ZIF-8 could form discrete water molecules or clusters, which makes ZIF-8 an ideal candidate for water channels in composite membranes. The CNTs enable efficient solar absorption for water evaporation and further accelerate the transportation of water due to their high surface area. A self-crosslinkable polyelectrolyte PCMVIMBr (poly[1-cyanomethyl-3-vinylimidazolium bromide]) was used for crosslinking carbon nanotubes (CNTs, light absorber) and *in situ* formed ZIF-8 particles to obtain composite membranes,[41,42] in which the interfacial

[a] *Collaborative Innovation Center for Advanced Organic Chemical Materials Co-constructed by the Province and Ministry, Ministry of Education Key Laboratory for the Synthesis and Application of Organic Functional Molecules and College of Chemistry and Chemical Engineering, Hubei University, Wuhan 430074, China. E-mail: dzhyue@hubu.edu.cn, zmh@maibox.gxnu.edu.cn*

[b] *Key Laboratory of Material Chemistry for Energy Conversion and Storage, Ministry of Education, Hubei Key Laboratory of Material Chemistry and Service Failure, School of Chemistry and Chemical Engineering, Huazhong University of Science and Technology, Wuhan 430074, China*

[c] *School of Chemistry and Pharmaceutical Sciences Guangxi Normal University, Key Laboratory for the Chemistry and Molecular Engineering of Medicinal Resources Guilin, 541004, China*

[d] *National "111" Center for Cellular Regulation and Molecular Pharmaceutics, Key Laboratory of Fermentation Engineering (Ministry of Education), Hubei Key Laboratory of Industrial Microbiology, Hubei University of Technology, Wuhan, 430068, China*

† Electronic supplementary information (ESI) available: Synthetic route of PCMVIMBr; PXRD, FT-IR and N 1s XPS curves of ZCP membranes; schematic illustration of the solar steam generation; and the details of the comparative literature. See DOI: https://doi.org/10.1039/d3ma00075c

‡ These authors contributed equally.

crosslinking of PCMVIMBr and ZIF-8 was achieved by the imidazole motifs of these two components. Besides, the high hydrophilicity of PCMVIMBr may improve the hydrophilic ability of the composite membranes. As such, the water evaporation enthalpy in these hybrid membranes for combination of these advantages was reduced, leading to high evaporation rates and antifouling ability.

## Experimental section

### Materials

2-Methylimidazole (2-MIM, 99%), $Zn(NO_3)_2{\cdot}6H_2O$ (Zinc, 98%), Zn-$(CH_3COO)_2{\cdot}2H_2O$ (98%), $ZnCl_2$ (98%), and dimethylformamide (DMF, 99.5%) were purchased from Sigma-Aldrich. PCMVIMBr was synthesized according to the previous work (Note S1, ESI†). Dimethylformamide (DMF), $NH_3$ solution (14 wt%), HCl solution (36.5 wt%), NaOH, Rhodamine B (RhB), and methyl blue (MB) were purchased from Sinopharm Chemical Reagent Co. Ltd (China). All the chemicals were at least analytical grade and used without further purification. Multi-walled carbon nanotubes (CNTs) with a diameter of 35–60 nm and length of *ca.* 30 μm were purchased from Chengdu Institute of Organic Chemistry (China). CNTs were ball-milled at 400 rpm for 6 h before being used and the length was reduced to 0.3–1 μm. Poly(vinylidene fluoride) (PVDF, diameter = 50 mm, pore size = 0.22 μm) filter membranes were bought from Shanghai Zuofei Experimental Equipment Co. Ltd (China). Wastewater was collected from Huxi river (Wuhan). Seawater was collected from the South China Sea (near to Hainan). An oil/water emulsion (dimethylpolysiloxane concentration = 10 000 ppm) was prepared as simulated wastewater.

### Synthesis of 1-cyanomethyl-3-vinyl-imidazolium bromide[41]

1-Vinylimidazole (10 g) and bromoacetonitrile (15 g) were dissolved in 125 mL of THF. After heating in an oil bath at 60 °C for 10 h, the precipitate, *i.e.*, 1-cyanomethyl-3-vinyl-imidazolium bromide, was vacuum-filtered, washed with THF three times, and vacuum-dried at 50 °C for 12 h.

### Synthesis of poly[1-cyanomethyl-3-vinyl-imidazolium bromide] (PCMVIMBr)

PCMVIMBr was synthesized according to the reported procedures.[41,43] 1-Cyanomethyl-3-vinyl-imidazolium bromide (10 g) and AIBN (0.08 g) were dissolved in 100 mL of DMSO, and heated at 60 °C for 12 h under a nitrogen atmosphere. Afterwards, the solution was dropped into excess THF (500 mL) and the precipitate (PCMVIMBr) was washed with THF three times and dried under vacuum at 50 °C for 16 h.

### Preparation of ZIF-8 hybrid membranes

Zinc precursor and PCMVIMBr were first dissolved in $H_2O$ (solution A), which is poured into solution B made by dissolving HMIM into $H_2O$.[44] The mixtures were then stirred for 6 hours for the crystallization of ZIF-8. Then the suspensions were ultrasonicated for 1 h and filtrated using PVDF filter membranes. Finally, after being treated in an $NH_3$ atmosphere (0.2 bar) at *ca.* 25 °C for 14 h, ZCP-*x* membranes were obtained, where *x* refers to the proportion of CNTs, *i.e.*, 5, 10, 15 20, 25 and 30 wt%.

### Interfacial solar steam generation[45]

A solar light simulator (CEL-S500L) was employed to conduct the interfacial steam generation experiment. Typically, the as-synthesized ZCP-*x* membranes with a diameter of *ca.* 40 mm were put on the surface of 2 cm-thick polystyrene foam, which was used as the thermal insulating layer and wrapped up by using hydrophilic silk to facilitate the diffusion of water to the membrane. The surface temperature of the membrane was constantly monitored by using an infrared thermal imaging camera (Dongmei, DM-I220). The water mass change was measured by using an electronic balance (Soptop, JA2003). The mass change of water was recorded in real time. The evaporation rate (kg $m^{-2}$ $h^{-1}$) and solar-to-vapor conversion efficiency (%) were calculated using eqn (S1) and (S2), respectively:

$$\text{Evaporation rate} = \Delta m/(S \times t) \quad \text{(S1)}$$

$$\text{Solar-to-vapor conversion efficiency} = m' \times h_{Lv}/P_{in} \quad \text{(S2)}$$

where $\Delta m$ is the mass change of water in 1 h (kg), $S$ is the area of the membrane ($m^2$), $t$ is the time of solar irradiation (1 h), $m'$ is the evaporation rate after subtracting the evaporation rate in the dark (kg $m^{-2}$ $h^{-1}$), $h_{Lv}$ is the latent heat of water vaporization (kJ $g^{-1}$), and $P_{in}$ is the incident light power on the absorber (kW $m^{-1}$). The temperature and relative humidity were *ca.* 30 °C and 50%, respectively.

The enthalpy values are calculated by the formula of $E_{equ} = E_w \times (R_w/R_m)$ according to the dark evaporation rate, where $E_{equ}$ is the evaporation enthalpy of water in the ZCP-20 membrane, $E_w$ is the enthalpy of bulk water, $R_m$ is the water evaporation rate of ZCP-20 in the dark, and $R_w$ is the dark evaporation rate of bulk water. Based on this formula, the enthalpy value of water in ZCP-20 is 0.99 kJ $g^{-1}$. The enthalpy values were calculated by integration of endothermic peaks of bulk water and the water in ZCP-20 based on the DSC results, and the enthalpy values were 2.339 kJ $g^{-1}$ and 1.01 kJ $g^{-1}$ respectively.

## Results and discussion

### Characterization of hybrid membranes

Fig. 1a shows the preparation scheme of the hybrid membranes. The CNTs were dispersed in PCMVIMBr and 2-methylimidazole aqueous solution, which was mixed with zinc ion solution. The mixed solution was stirred for 1 hour at 25 °C. In this process, ZIF-8 particles were synthesized *in situ*. The mixed solution was vacuum filtrated onto poly(vinylidene fluoride) (PVDF) membranes (5 cm diameter), dried at room temperature for 2 hours, and then the hybrid membranes were treated in an $NH_3$ atmosphere (0.2 bar) at 25 °C for 14 hours. The as-prepared hybrid membranes were named ZCP-*x*, abbreviated as ZCP-*x* where *x* denotes the mass content of CNTs in these hybrid membranes. The diameter of these membranes is 4 cm due to the limitation of the filters (Fig. S3, ESI†). In addition, the mass ratio of ZIF-8 to PCMVIMBr in all hybrid membranes is maintained at 10 : 3.4

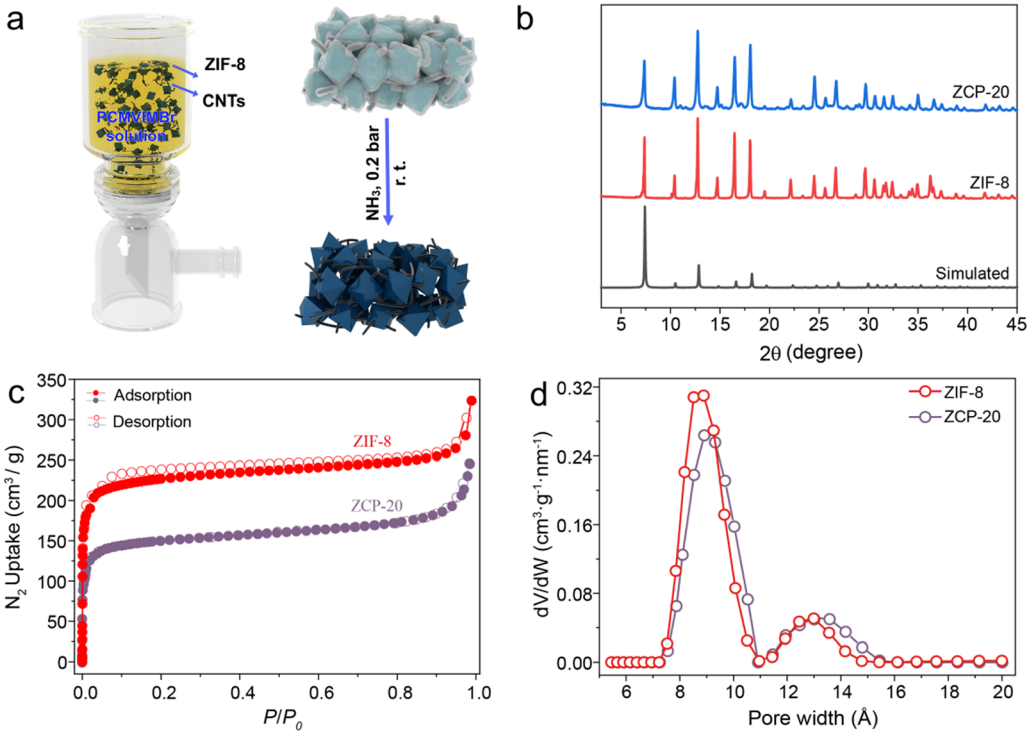


Fig. 1 (a) Scheme of ZCP-*x* membranes and (b–d) their XRD, $N_2$ isotherm curves and Pore width of ZIF-8 and ZCP-20.

(Table S1, ESI†). After $NH_3$ treatment, the cyano groups of PCMVIMBr were crosslinked into triazine rings to form polymer shells, which would bind CNTs and ZIF-8 particles together. In this synthetic process, the imidazole ring in PCMVIMBr may

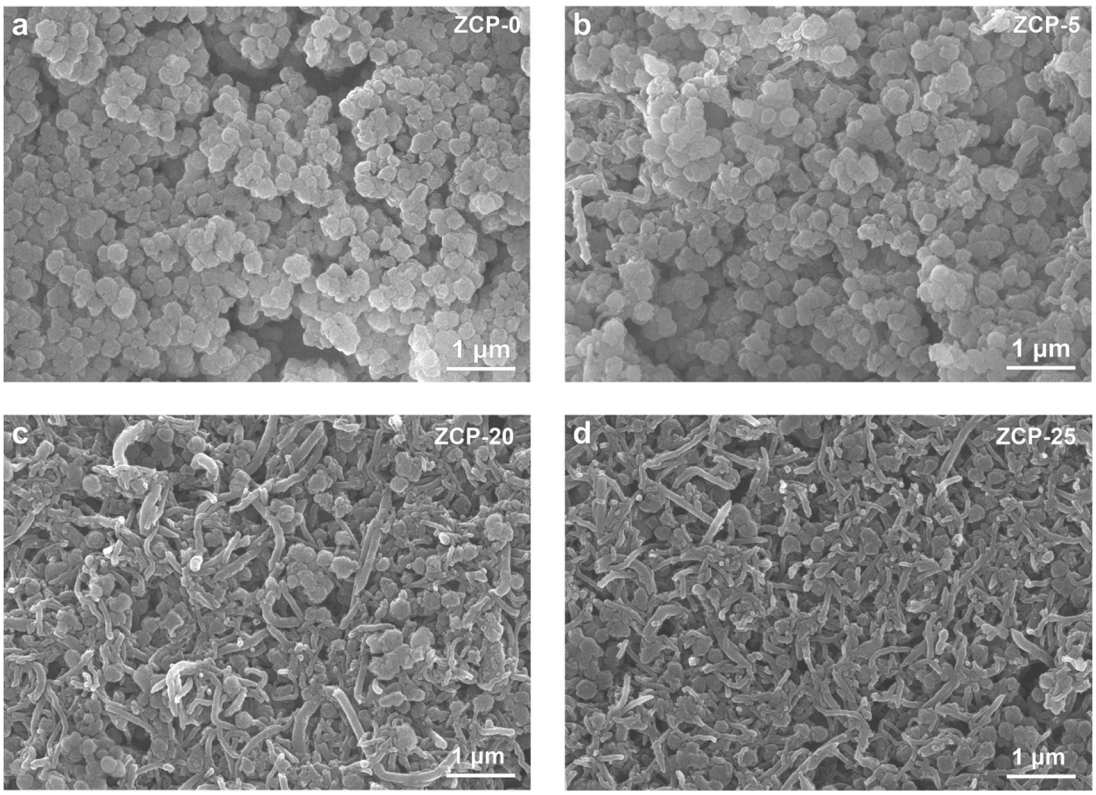


Fig. 2 The SEM images of ZCP-*x* (*x* represents 0, 5, 20, and 25, which refers to the CNT percentage in the membranes).

partly replace the 2-methylimidazole linkers to coordinate Zn ions to give high affinity to ZIF-8 particles. The membranes were used for water evaporation to give a steam evaporation rate of up to 2.48 kg $m^{-2}$ $h^{-1}$.

The intrinsic porosity of ZIF-8 was characterized by the $N_2$ adsorption isotherm and pore size distribution. The BET surface area is about 1000 $m^2$ $g^{-1}$ and the cavities are about 8–14 Å in diameter, consistent with the literature values (Fig. 1c and d). As shown in Fig. 1b, the PXRD (powder X-ray diffraction) pattern of ZCP-20 confirms that the crystallinity of ZIF-8 is retained. Infrared spectroscopy shows peaks around 1400 and 1300 $cm^{-1}$ for ZIF-8, which are assigned to stretching vibration of the imidazolate ring. These bands are also observed for the ZCP membranes, consistent with the preservation of ZIF-8 after the crosslinking of PCMVIMBr (Fig. S4, ESI†). Meanwhile, the representative adsorption bands around 1692 and 1623 $cm^{-1}$ in the crosslinked PCMVIMBr are assigned to stretching vibration and symmetrical stretching vibration of the triazine ring N–C═N motif.[41]

The SEM images of the ZCP-*x* membranes (Fig. 2a–d) reveal the structures of compactly assembled ZIF-8 particles and CNTs. As displayed in Fig. 2a, ZIF-8 particles in ZCP-0 show uniform size of about 200 nm. With the content of CNTs increased to 25 wt%, CNTs are still uniformly dispersed in the hybrid membranes. Furthermore, ZCP-*x* membranes show a homogeneous distribution of CNTs on the surface roughened by the ZIF-8 particles (Fig. 2b–d). These SEM images confirmed the crosslinking effect of PCMVIMBr with ZIF-8 surfaces. The XPS characterizations found the relative contents of $sp^2$ C, C–O–C, –C≡N and N–C═N in ZCP-20 to be 79%, 5%, 1% and 3%, respectively, which originate from those of ZIF-8 or crosslinked PCMVIMBr (Fig. 3b, c and Fig. S5, ESI†). Similarly, the relative content of C═O/C–N is calculated, which can be attributed to CNTs, ZIF-8 and PCMVIMBr (Fig. 3a and b).[46] Thus, the XPS characterization also confirms the integrity of ZIF-8, PCMVIBr and CNTs in the hybrid membrane.

### Variation of surface temperature

The sunlight absorbability of the ZCP-20 membrane in the visible and infrared regions was measured by UV-vis-NIR spectroscopy (Fig. 4a). The ZCP-20 membrane shows a broadband absorption of solar irradiation of up to 99%, much higher than the absorption of ZIF-8 and ZCP-0 membranes. The higher optical absorption of ZCP-20 is due to the presence of well-distributed CNTs. Upon visible and infrared light irradiation, CNTs are excited to perform an electronic transition from the highest occupied molecular orbital[48] to the lowest unoccupied molecular orbital.[47] Owing to this transition, an electron–phonon coupling induces the transfer of energy from the excited electrons to the atomic lattice vibration, resulting in a heating effect. The uniform distribution of CNTs in the ZCP-20 membrane extends the residence time of incident light

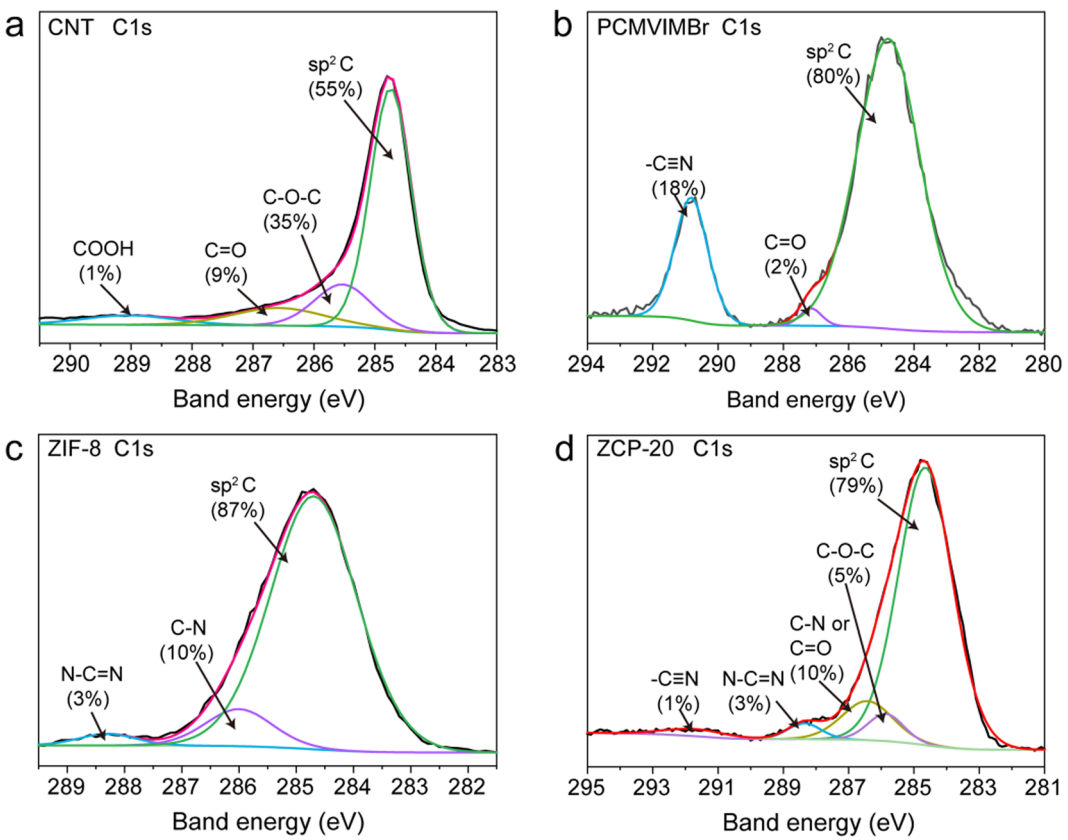


Fig. 3 The high-resolution C1s XPS spectra of (a) CNTs, (b) PCMVIMBr, (c) ZIF-8 and (d) ZCP-20.

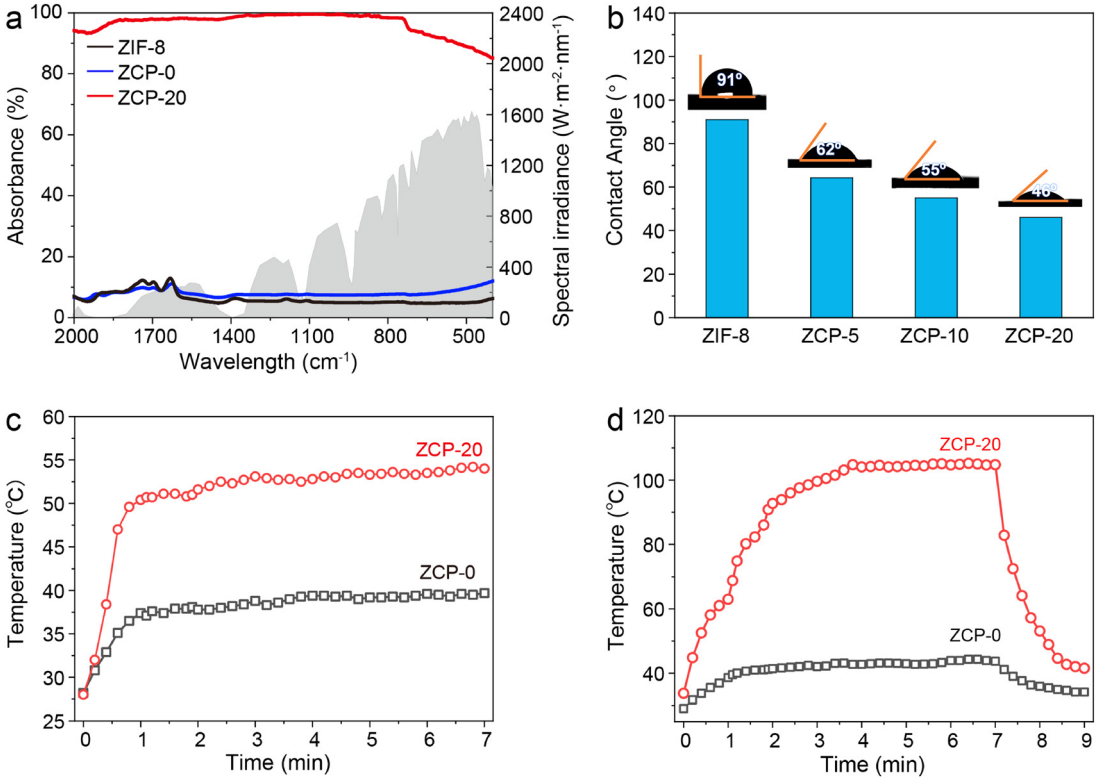


Fig. 4 (a) The Vis-NIR absorption spectra of ZIF-8, ZCP-0 and ZCP-20 membranes. (b) Contact angle images of ZIF-8, ZCP-5, ZCP-10 and ZCP-20 membranes. (c and d) Surface temperatures over different times of the ZCP-0 membrane and ZCP-20 membrane.

and thereby improves the visible light absorption *via* light scattering.

Besides, the excellent sunlight absorbability and low thermal conductivity (0.1237 W $m^{-1}$ $K^{-1}$) of the ZCP-20 membrane could effectively reduce the conductive heat loss. As a proof of concept, under 1 kW $m^{-2}$ irradiation, the surface temperature of the ZCP-20 membrane in the wet state increases rapidly to 47 °C within 1 min, then gradually goes up to 53 °C, and maintains the temperature steadily upon extending the irradiation time (Fig. 4c, red line and Fig. 5a). However, the ZCP-0 membrane shows a relatively low surface temperature increase to 40 °C (Fig. 4c, black line). While in the dry state, the temperature of ZCP-20 increases to 104 °C in 3 min (Fig. 4d, red line and Fig. 5b) and when the light source is blocked, the temperature immediately returns to

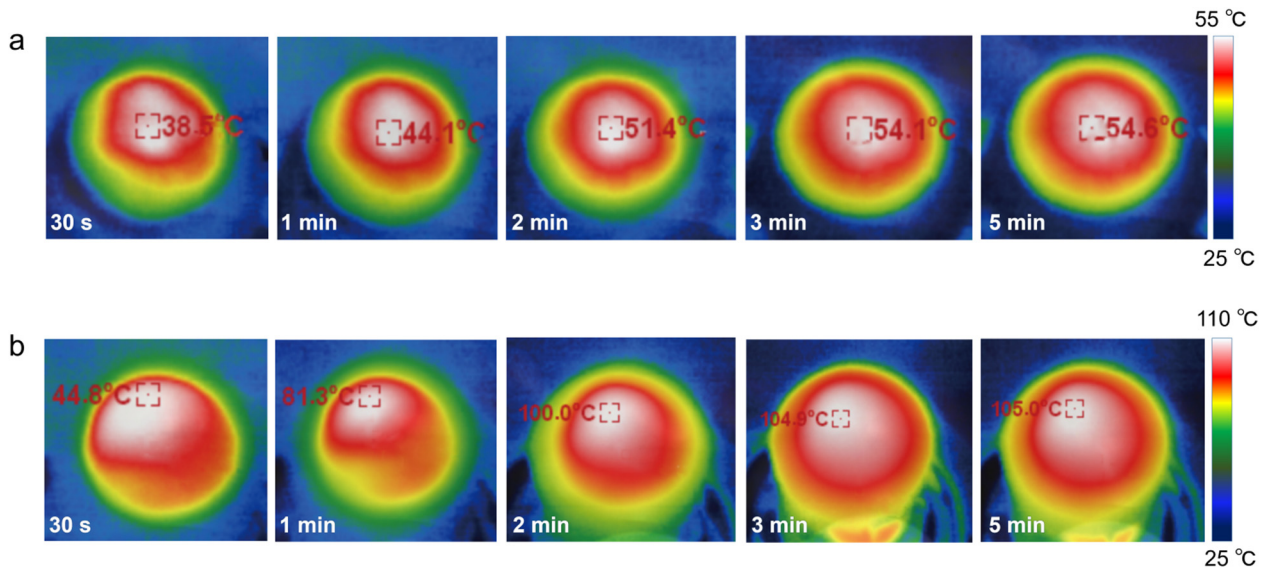


Fig. 5 Infrared images of ZCP-20 in the wet state (a) and in the dry state (b) over different times.

40 °C. In contrast, the temperature of the ZCP-0 membrane could only reach 42 °C in the dry state (Fig. 4d, black line). The above experimental results demonstrate the good performance of the ZCP-20 membrane in transforming the harvested solar energy to thermal energy. As shown in Fig. 4b, the contact angle of ZCP-20 is 46°, which is lower than those of ZCP-0 (91°), ZCP-10 (55°) and ZCP-5 (62°). These results suggest that the ZCP-20 membrane shows providential hydrophilicity in comparison with control membranes, which is likely due to the combination of hydrophilic PCMVIMBr with the nanostructures of ZIF-8 and CNTs.

### Water evaporation

The water evaporation performance under 1 kW $m^{-2}$ solar irradiation of ZCP-20 was investigated by using a lab-made, real-time measurement system (Fig. S6, ESI†). The mass change of water due to the steam generation was measured by using an electronic analytical balance. The water mass of all samples decreases relatively linearly (Fig. 6a). After 60 min, the mass loss of the ZCP-20 membrane reaches 2.48 kg $m^{-2}$ $h^{-1}$, much higher than those of the PVDF membrane (0.49 kg $m^{-2}$ $h^{-1}$), CP-20 (CNTs@PCMVIMBr-20) membrane (1.68 kg $m^{-2}$ $h^{-1}$), and ZCP-0 membrane (0.69 kg $m^{-2}$ $h^{-1}$). In addition, as the CNT content increases from 5 to 20 wt%, the evaporation rate goes up from 1.08 to 2.48 kg $m^{-2}$ $h^{-1}$ (Fig. 6b). This is because the presence of more CNTs improves the light absorption. However, the evaporation rate slightly decreases down to 1.74 kg $m^{-2}$ $h^{-1}$ after further increasing the content of CNTs to 30 wt%, likely attributed to the retardancy of water transportation. The solar-to-vapor conversion efficiencies show similar trends (Fig. 6b). The solar-to-vapor conversion efficiency of ZCP-20 is 67.1%, which is the highest among those of ZCP-*x* membranes (*x* represents 0, 5%, 10%, 15%, 25%, and 30%). As shown in Fig. 6c, the water evaporation enthalpies calculated from the dark evaporation rates are 2.32 kJ $g^{-1}$ for water, 0.99 kJ $g^{-1}$ for the ZCP-20 membrane, 1.18 kJ $g^{-1}$ for the ZCP-0 membrane, and 1.24 kJ $g^{-1}$ for the CP-20 (CNTs@PCMVIMBr-20) membrane. Equivalent enthalpies of ZCP-20 and ZCP-0 were reduced by 56% and 50%, respectively, compared with that of pure water. The reduction of the equivalent enthalpy of the CP-20 membrane compared to that of bulk water is echoed in the conjectural water transmission mechanism. Additionally, the enthalpy change of ZCP-20 measured by DSC (Fig. 6d) is calculated to be 1.01 kJ $g^{-1}$, which is consistent with the value calculated by experiments (0.99 kJ $g^{-1}$). This excellent performance of ZCP-20 can be attributed to the through channels and the cage-like pores of ZIF-8, which prompt bulk water to form discrete molecules or clusters (Fig. 6e). Coupled with suitable hydrophobic pores, the water enthalpy was reduced effectively. Meanwhile, the three-dimensional structure of CNTs with a high specific surface area can facilitate the transportation of water, resulting in the further reduction of the evaporation enthalpy. After water evaporation, the structure of ZIF-8 in the ZCP-20 membrane remained almost unchanged (Fig. S8, ESI†).

The interfacial solar steam generation using ZCP-*x* membranes is illustrated in Fig. 7a. The solar-thermal steaming performance of the ZCP-20 membrane is superior compared to those of the state-of-the art materials in terms of evaporation rate (Fig. 7b and Table S2, ESI†). Besides, the ZCP-20 membrane shows stable performance (*ca.* 2.29–2.48 kg $m^{-2}$ $h^{-1}$, Fig. 7c) and the membrane's structure in 20 h continuous solar-thermal evaporation. The high recyclability could be sustained to

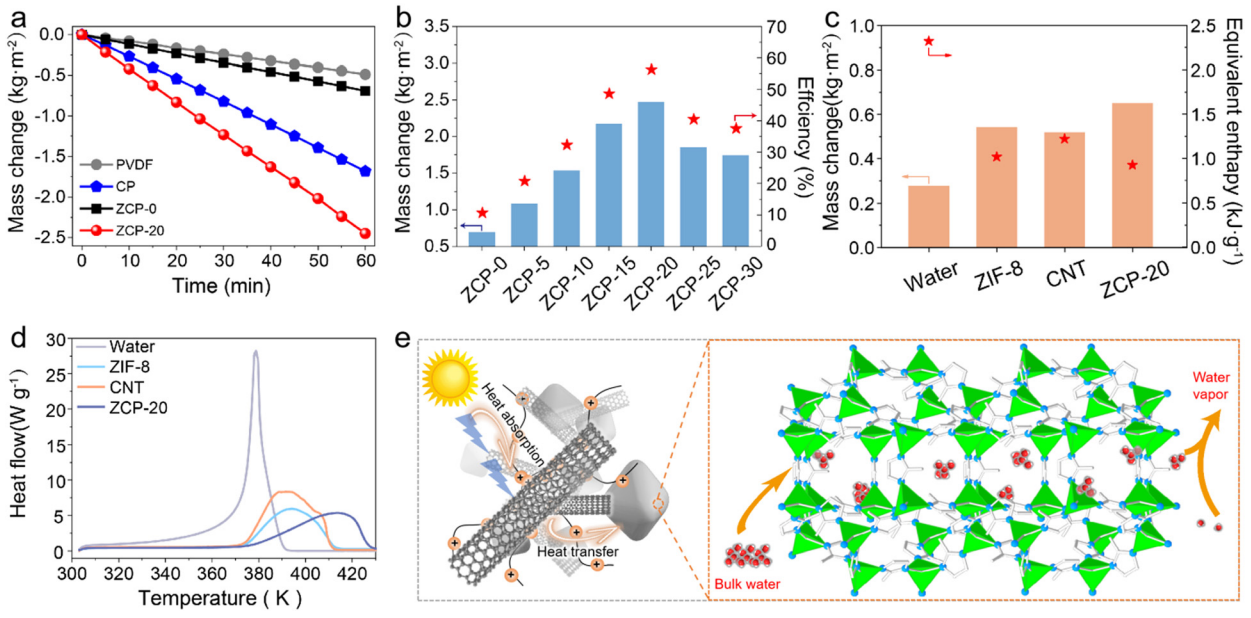


Fig. 6 (a) Cumulative mass changes of water under 1 kW $m^{-2}$ irradiation using PVDF, CP, ZCP-0 and ZCP-20 membranes. (b) Evaporation rates and solar-to-vapor conversion efficiencies of ZCP-*x* membranes. (c) Cumulative mass changes of water without absorbers (noted as "Water"), ZIF-8, CNT and ZCP-20 membranes and their equivalent enthalpies. (d) The DSC curves of water, ZIF-8, CNTs and ZCP-20 membranes. (e) The illustration of heat transmission and the formation of discrete water molecules and water clusters.

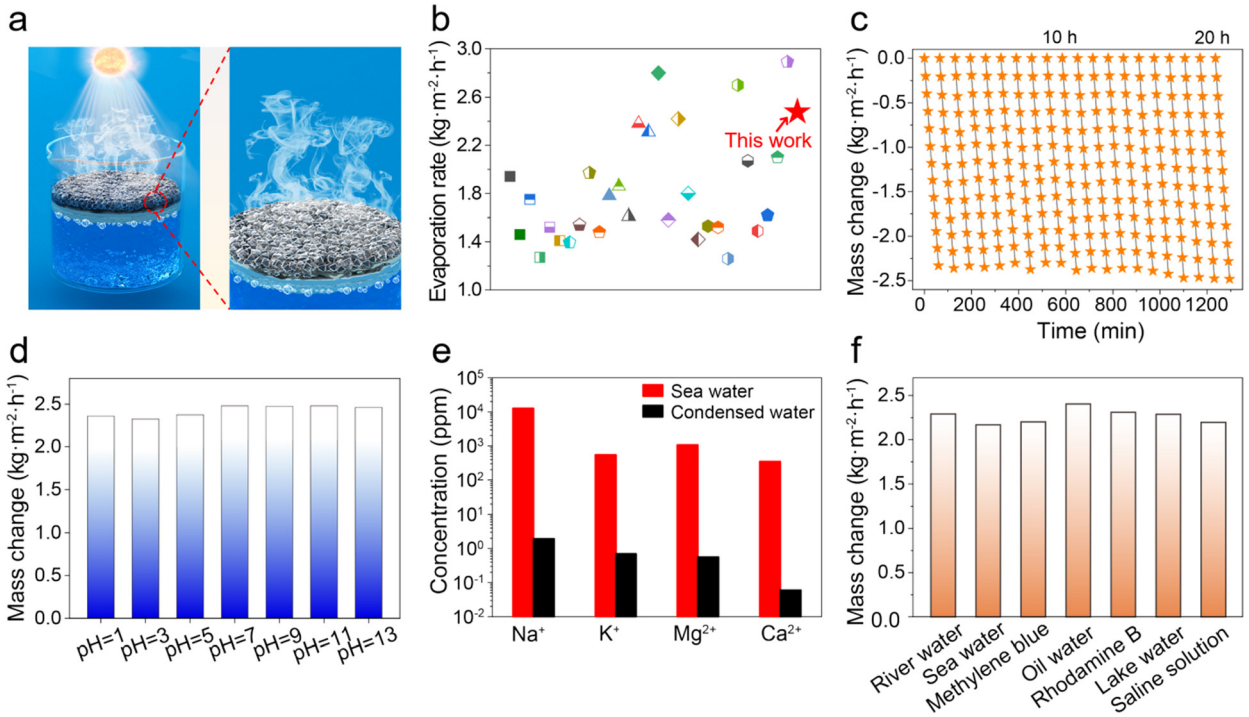


Fig. 7 (a) Schematic illustration for interfacial solar steam generation using ZCP-*x* membranes and (b) comparison of the water evaporation rate of ZCP-20 with those of reported photothermal materials (Table S2, ESI†). (c) Cumulative mass changes of the ZCP-20 membrane for 20 h. (d) Evaporation rates of the ZCP-20 membrane using water of different pH. (e) Ionic concentrations of seawater and condensed water. (f) Evaporation rates using other water sources.

72 hours according to the evaporation performance interval of 12 hours (Fig. S9, ESI†). Also, the ZCP-20 membrane was slightly activated in the continuous evaporation process and the evaporation rate shows a slight increase to 2.48 kg $m^{-2}$ $h^{-1}$ as the evaporation time is increased. The ZCP-20 is tolerant to acidic and basic water, as the evaporation rates of the ZCP-20 membrane are maintained around 2.36–2.46 kg $m^{-2}$ $h^{-1}$ for solar-steaming pH = 1 and 13 solutions (Fig. 7d). More importantly, with the merits of acid/base stabilities and being metal-free, the ZCP-20 membrane matches the state-of-the-art photothermal materials, including $ZrB_2$@ASCF ($ZrB_2$@aluminium silicate ceramic fibreboard, 2.07 kg $m^{-2}$ $h^{-1}$),[7] nanoporous black Au film (1.51 kg $m^{-2}$ $h^{-1}$),[48] PI/MXene hybrid aerogel (polyimide/MXene hybrid aerogel 1.24 kg $m^{-2}$ $h^{-1}$),[49] TPC@CB (thermoplastic polyurethane–carbon nanotubes@carbon black, 1.80 kg $m^{-2}$ $h^{-1}$),[50] CNT–GO@BC (bacterial cellulose, 1.85 kg $m^{-2}$ $h^{-1}$),[22] and polydimethylsiloxane/carbon nanotubes/poly(vinylidene fluoride) membrane (PDMS/CNT/PVDF, 1.43 kg $m^{-2}$ $h^{-1}$).[21]

Interfacial solar-driven vapor generation experiments of ZCP-20 membrane using seawater, river water, oil/water emulsion, lake water, and organic dye-containing water (including RhB and MB) were also investigated under 1 kW $m^{-2}$ irradiation. The membrane's excellent performance is maintained in solar thermal desalination of real seawater and clean water production from the other sources (Fig. 7e and f). The evaporation rate of seawater is up to 2.16 kg $m^{-2}$ $h^{-1}$ and the ZCP-20 membrane shows a good self-cleaning ability (Fig. S7, ESI†). After desalination, the ionic concentration of the condensed water decreases from 12 742.9 ppm to 1.9 ppm for $Na^+$, from 546.3 ppm to 0.7 ppm for $K^+$, from 1065 ppm to 0.6 ppm for $Mg^{2+}$, and from 348.2 ppm to 0.06 ppm for $Ca^{2+}$ (Fig. 7e). Importantly, the collected fresh water satisfies the standard of healthy drinkable water as defined by the World Health Organization (*i.e.*, $Na^+ <$ 1000 ppm).[51] The condensed water from the organic dye-containing water is colorless and shows a negligible absorption (Fig. 8a). When the oil/water emulsion is tested, oil droplets are hardly found in the condensed water (Fig. 8b–d). Overall, the removal efficiency of metallic ions, oil and organic dyes in water is over 99.9%; meanwhile, the evaporation rate of ZCP-20 remains as 2.16–2.40 kg $m^{-2}$ $h^{-1}$ (Fig. 7d), suggesting the high performance of ZCP-20 in seawater desalination and lake water treatment.

## Conclusions

ZCP membranes were prepared by filtering *in situ* formed ZIF-8 nanoparticles with CNTs and PCMVIMBr on PVDF, followed by self-crosslinking of PCMVIMBr under mild conditions. This facile strategy is conducive to wrapping neighbouring ZIF-8 particles and CNTs by PCMVIMBr without blemishing their structure. The formation of scattered water molecules or clusters in the nanochannels and cage nanopores of ZIF-8 promotes the reduction of the water evaporation enthalpy of the ZCP-20 membrane by 56%, compared to that of bulk water. Thanks to the broadband and good sunlight absorption, high conversion efficiency, low thermal conductivity and reduced water

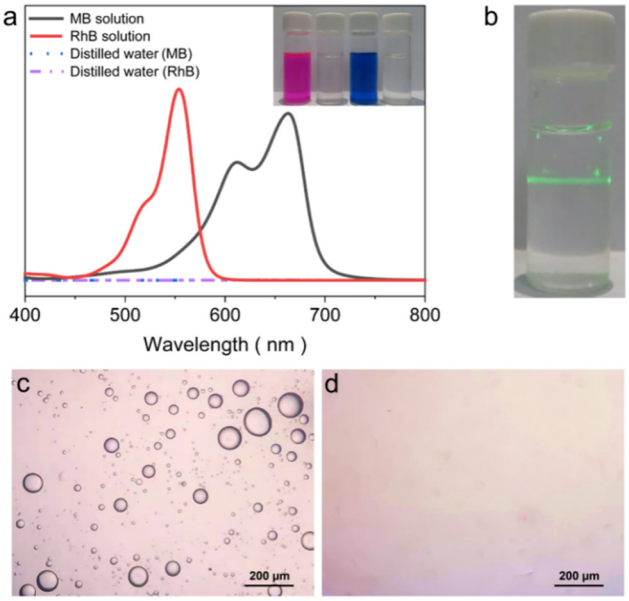


Fig. 8 (a) The UV-vis spectra and the colours comparison (inset) of RhB or MB-polluted water and freshwater. (b) Tyndall effect of oil/water emulsion. Optical images of (c) the oil/water emulsion and (d) freshwater collected from the emulsion.

evaporation enthalpy, the ZCP-20 membrane exhibits an outstanding evaporation rate of 2.48 kg $m^{-2}$ $h^{-1}$ with excellent long-term durability under 1 kW $m^{-2}$ irradiation. The resultant ZCP-20 hybrid membrane displays an excellent stability in strong acidic or basic solutions and maintains high performance in lake water treatment. We believe that this work provides a facile strategy to prepare flexible, robust, hybrid photothermal membranes with high solar-thermal evaporation rates and efficiencies, which could be excellent candidates for solar steam generation and seawater desalination.

## Author contributions

This manuscript was written through contributions of all the authors. All the authors have given approval to the final version of the manuscript.

## Conflicts of interest

There are no conflicts to declare.

## Acknowledgements

Z. D. acknowledges financial support from the National Natural Science Foundation of China for Distinguished Young Scholars (No. 22101077) and financial support from the Youth Foundation of Hubei Province (No. ZRMS2021000795) and the "Chu-Tian Scholar" Program of Hubei Province. M. H. Z. acknowledges support from the National Natural Science Foundation of China (No. 22171075), Guangxi Province (No. 2017GXNSFDA198040), and the BAGUI talent program (No. 2019AC26001).

## Notes and references

1 B. Luo, J. Wen, H. Wang, S. Zheng, R. Liao, W. Chen, O. Mahian and X. Li, *Energy Environ. Mater.*, 2022, **0**, 1–11.
2 B. Peng, Q. Lyu, Y. Gao, M. Li, G. Xie, Z. Xie, H. Zhang, J. Ren, J. Zhu, L. Zhang and P. Wang, *ACS Appl. Mater. Interfaces*, 2022, **14**, 16546–16557.
3 R. Zhu, D. Wang, Y. Liu, M. Liu and S. Fu, *Chem. Eng. J.*, 2022, **433**, 133510.
4 P. Si, Q. Wang, H. Kong, Y. Li and Y. Wang, *ACS Appl. Mater. Interfaces*, 2022, **14**, 19652–19658.
5 P. Wu, X. Wu, Y. Wang, H. Xu and G. Owens, *Chem. Eng. J.*, 2022, **435**, 134793.
6 S. Meng, C. Y. Tang, J. Jia, J. Yang, M. B. Yang and W. Yang, *Adv. Energy Mater.*, 2022, **12**, 122200087.
7 S. Ai, T. J. Li, Y. Z. Chen, C. Y. He, B. H. Liu, G. Liu and X. H. Gao, *Chem. Eng. J.*, 2022, **431**, 134333.
8 C. Li, S. Cao, J. Lutzki, J. Yang, T. Konegger, F. Kleitz and A. Thomas, *J. Am. Chem. Soc.*, 2022, **144**, 3083–3090.
9 M. X. Guo, J. B. Wu, H. Y. Zhao, F. H. Li and F. Q. Min, *Int. J. Energy Res.*, 2021, **45**, 10599–10608.
10 X. l Yan, S. Z. Lyu, X. Q. Xu, W. B. Chen, P. N. Shang, Z. F. Yang, G. Zhang, W. H. Chen, Y. P. Wang and L. Chen, *Angew. Chem., Int. Ed.*, 2022, **61**, e202201900.
11 X. Li, W. Xu, M. Tang, L. Zhou, B. Zhu, S. Zhu and J. Zhu, *Proc. Natl. Acad. Sci. U. S. A.*, 2016, **113**, 13953–13958.
12 Q. Ma, Q. He, P. Yin, H. Cheng, X. Cui, Q. Yun and H. Zhang, *Adv. Mater.*, 2020, **32**, e2003720.
13 Z. C. Xiong, Y. J. Zhu, D. D. Qin, F. F. Chen and R. L. Yang, *Small*, 2018, **14**, e1803387.
14 H. Kou, Z. Liu, B. Zhu, D. K. Macharia, S. Ahmed, B. Wu, M. Zhu, X. Liu and Z. Chen, *Desalination*, 2019, **462**, 29–38.
15 L. Li, L. Zang, S. Zhang, T. Dou, X. Han, D. Zhao, Y. Zhang, L. Sun and Y. Zhang, *J. Taiwan Inst. Chem. Eng.*, 2020, **111**, 191–197.
16 X. Li, C. Guan, X. Gao, X. Zuo, W. Yang, H. Yan, M. Shi, H. Li and M. Sain, *ACS Appl. Mater. Interfaces*, 2020, **12**, 35493–35501.
17 G. Chen, Z. Jiang, A. Li, X. Chen, Z. Ma and H. Song, *J. Mater. Chem. A*, 2021, **9**, 16805–16813.
18 F. Yang, J. Chen, Z. Y. Ye, D. W. Ding, N. V. Myung and Y. D. Yin, *Adv. Funct. Mater.*, 2021, **31**, 2006294.
19 Z. Sun, Z. Li, W. Li and F. Bian, *Cellulose*, 2019, **27**, 481–491.
20 W. Li, X. F. Li, J. Liu and M. J. Zeng, *ACS Appl. Mater. Interfaces*, 2021, **13**, 22845–22854.
21 J. Huang, Y. Hu, Y. Bai, Y. He and J. Zhu, *Desalination*, 2020, **489**, 114529.
22 M. Jin, Z. Wu, F. Guan, D. Zhang, B. Wang, N. Sheng, X. Qu, L. Deng, S. Chen, Y. Chen and H. Wang, *ACS Appl. Mater. Interfaces*, 2022, **14**, 12284–12294.
23 J. D. Yi, R. Xie, Z. L. Xie, G. L. Chai, T. F. Liu, R. P. Chen, Y. B. Huang and R. Cao, *Angew. Chem., Int. Ed.*, 2020, **59**, 23641–23648.
24 Q. Ma, P. Yin, M. Zhao, Z. Luo, Y. Huang, Q. He, Y. Yu, Z. Liu, Z. Hu, B. Chen and H. Zhang, *Adv. Mater.*, 2019, **31**, e1808249.
25 C. Song, Z. Jiang, X. Gu, H. Li and J. Shi, *J. Colloid, Interface Sci.*, 2022, **616**, 709–719.

26 X. Ma, Z. Deng, Z. Li, D. Chen, X. Wan, X. Wang and X. Peng, *J. Mater. Chem. A*, 2020, **8**, 22728–22735.
27 C. Song, M. S. Irshad, Y. Jin, J. Hu and W. Liu, *Desalination*, 2022, **544**, 116125.
28 X. Han, L. V. Besteiro, C. S. L. Koh, H. K. Lee, I. Y. Phang, G. C. Phan-Quang, J. Y. Ng, H. Y. F. Sim, C. L. Lay, A. Govorov and X. Y. Ling, *Adv. Funct. Mater.*, 2021, **31**, 2008904.
29 X. Ma, W. Fang, Y. Guo, Z. Li, D. Chen, W. Ying, Z. Xu, C. Gao and X. Peng, *Small*, 2019, **15**, e1900354.
30 C. Song, X. Chen, R. Hao, D. Cai, X. Zhu, H. Liu, J. Chen and W. Liu, *Sustainable Energy Fuels*, 2021, **5**, 4126–4132.
31 Z. Yin, Y. Zhao, S. Wan, J. Yang, Z. Shi, S. Peng, M. Chen, T. Xie, T. Zeng, O. Yamamuro, M. Nirei, H. Akiba, Y. Zhang, H. Yu and M. Zeng, *J. Am. Chem. Soc.*, 2022, **144**, 13021–13025.
32 H. N. Abdelhamid and A. P. Mathew, *Chem. Eng. J.*, 2021, **426**, 131733.
33 H. Deng, C. J. Doonan, H. Furukawa, R. B. Ferreira, J. Towne, C. B. Knobler, B. Wang and O. M. Yaghi, *Science*, 2010, **327**, 846–850.
34 X. Kong, H. Deng, F. Yan, J. Kim, J. Swisher, B. Smit, O. M. Yaghi and J. A. Reimer, *Science*, 2013, **341**, 882–885.
35 Z. Dong, Y. Sun, J. Chu, X. Zhang and H. Deng, *J. Am. Chem. Soc.*, 2017, **139**, 14209–14216.
36 H. N. Abdelhamid, D. Georgouvelas, U. Edlund and A. P. Mathew, *Chem. Eng. J.*, 2022, **446**, 136614.
37 M. Hayashi, D. T. Lee, M. D. D. Mello, J. A. Boscoboinik and M. Tsapatsis, *Angew. Chem., Int. Ed.*, 2021, **60**, 9316–9320.
38 H. N. Abdelhamid and A. P. Mathew, *Coord. Chem. Rev.*, 2022, **451**, 214263.
39 T. Wu, J. Dong, K. De France, P. Zhang, X. Zhao and Q. Zhang, *Chem. Eng. J.*, 2020, **395**, 124927.
40 F. Hillman, M. R. A. Hamid, P. Krokidas, S. Moncho, E. N. Brothers, I. G. Economou and H. K. Jeong, *Angew. Chem., Int. Ed.*, 2021, **60**, 10103–10111.
41 Z. Dong, C. Zhang, H. Peng, J. Gong, H. Wang, Q. Zhao and J. Yuan, *Mater. Horiz.*, 2020, **7**, 2683–2689.
42 P. Cao, L. Zhao, Z. Yang, P. Yuan, Y. Zhang, Q. Li and Q. Li, *ACS Appl. Mater. Interfaces*, 2021, **4**, 8906–8912.
43 Q. Zhao, J. W. Dunlop, X. Qiu, F. Huang, Z. Zhang, J. Heyda, J. Dzubiella, M. Antonietti and J. Yuan, *Nat. Commun.*, 2014, **5**, 4293.
44 C. Ji, J. Zhang, R. Jia, W. Zhang, L. Lv and B. Pan, *Chem. Eng. J.*, 2021, **414**, 128812.
45 C. Song, L. Hao, B. Zhang, Z. Dong, Q. Tang, J. Min, Q. Zhao, R. Niu, J. Gong and T. Tang, *Sci. China Mater.*, 2020, **63**, 779–793.
46 Y. Wen, X. Chen and E. Mijowska, *Chemistry*, 2020, **26**, 16328–16337.
47 G. Hu, Y. Cao, M. Huang, Q. Wu, K. Zhang, X. Lai, J. Tu, C. Tian, J. Liu, W. Huang and L. Ding, *Energy Technol.*, 2019, **8**, 1900721.
48 Y. Zhang, Y. Wang, B. Yu, K. Yin and Z. Zhang, *Adv. Mater.*, 2022, **34**, e2200108.
49 Z. Zheng, H. Liu, D. Wu and X. Wang, *Chem. Eng. J.*, 2022, **440**, 135862.
50 S. Li, F. Qiu, Y. Xia, D. Chen and X. Jiao, *ACS Appl. Mater. Interfaces*, 2022, **14**, 19409–19418.
51 J. L. Wang, W. Wang, J. G. Li, X. Y. Mu, X. Y. Yan, Z. Wang, J. Su, T. Lei and C. Wang, *ACS Appl. Mater. Interfaces*, 2021, **13**, 45944–45956.